DOI 10.1007/s11237-016-9470-x
*Theoretical and Experimental Chemistry, Vol. 52, No. 4, September, 2016 (Russian Original Vol. 52, No. 4, July-August, 2016)*

# EFFECT OF THE STRUCTURE AND ACIDITY OF MICRO-MESOPOROUS ALUMOSILICATES ON THEIR CATALYTIC ACTIVITY IN CUMENE CRACKING

**R. Yu. Barakov,[1] N. D. Shcherban,[1] P. S. Yaremov,[1] Yu. G. Voloshyna,[2] M. M. Krylova,[2] V. V. Tsyrina,[1] and V. G. Ilyin[1†]**

UDC 544.723.21; 544.478.02; 665.64

*Micro-mesoporous alumosilicates derived from zeolite ZSM-5 were obtained in dual template reaction media and in the presence of dual functional templates. It was shown that aluminosilicates with 0.15-0.25 zeolitization exhibit high catalytic activity in cumene cracking, approaching the activity of ZSM-5 and superior to ZSM-5 in total selectivity relative to the major products (propylene and benzene). Greater oligomerization of propylene is observed with increasing micropore volume and concentration of strong acid sites in the alumosilicates along with increased cumene conversion.*

***Key words:*** *micro-mesoporous alumosilicate, dual template synthesis, dual functional template, porosity, acidity, catalytic cumene cracking.*

In recent years, there has been considerable work on the development of micro-mesoporous materials (or so-called hierarchical porous materials), including micro-mesoporous alumosilicates (MMAS) [1]. These materials combine to some extent the properties of zeolites (Zt) and mesoporous molecular sieves (MMS), in particular, they contain strong acid sites as well as mesopores, which facilitate enhancement of the rates of diffusion processes and greater accessibility of the catalytically active sites for reagent molecules [2]. As a consequence, MMAS display high catalytic activity in the cracking and isomerization of hydrocarbons and the conversion of bulky organic molecules with kinetic diameter greater than the zeolite pore diameter (0.3-1 nm), including alkylation, acylation, aldol condensation, and esterification reactions [3].

Promising approaches to the preparation of MMAS involve dual template synthesis in the presence of molecular and micellar templates responsible for the formation of zeolites and MMS, respectively [4] and the use of dual functional templates [5]. The hydrophilic part of a dual functional template consisting of 2-8 ammonium groups acts as a structure-directing agent

[1]L. V. Pisarzhevskii Institute of Physical Chemistry, National Academy of Sciences of Ukraine, Prospekt Nauky, 31, Kyiv 03028, Ukraine. E-mail: barakovchem07@rambler.ru.
[2]Institute of Bioorganic Chemistry and Petrochemistry, National Academy of Sciences of Ukraine, Vul. Murmans'ka, 1, Kyiv 02660, Ukraine. E-mail: yule.v444@gmail.com.
[†]Deceased.

Translated from Teoreticheskaya i Éksperimental'naya Khimiya, Vol. 52, No. 4, pp. 213-221, July-August, 2016. Original article submitted July 19, 2016; revision submitted July 25, 2016.

 

TABLE 1. Synthesis Conditions and Structural Characteristics of Prepared Samples

| Sample | Template | HTT of RM | | pH of RM before HTT | $V_{micro}\cdot10^{-2}$, $cm^3/g$ | $V_{meso}$, $cm^3/g$ | $D_{meso}$, nm | $S_{meso}$, $m^2/g$ | $S_{BET}$, $m^2/g$ |
|---|---|---|---|---|---|---|---|---|---|
| | | $T$, °C | τ, days | | | | | | |
| 1-100 | TPAOH, CTACl | 100 | 3 | 12.9 | – | 0.57 | 2.3 ± 0.4 | 1240 | 1245 |
| 2-100 | | 100 | 6 | 12.9 | 0.90[a] | 0.50 | 2.4 ± 0.4 | 815 | 960 |
| 3-100 | | 100 | 3 | 11.7 | 2.90 | 0.55 | 2.6 ± 0.3 | 770 | 855 |
| 4-100 | | 100 | 3 | 11.0 | 0.30 | 0.60 | 2.7 ± 0.2 | 950 | 995 |
| 1-130 | $C_{8-6-8}Br_2$ | 130 | 6 | 11.0 | 13.5 | 0.41 | 11.0 ± 2.0 | 175 | 500 |
| 2-130 | $C_{8-6-8}Br_2$, CTAB | 130 | 6 | 11.2 | 11.9 | 0.30 | 5.6 ± 0.6 | 250 | 540 |
| 3-130 | $C_{16-6-6}Br_2$ | 130 | 6 | 10.5 | 10.8 | 0.26 | 2.5 ± 1.0 | 240 | 505 |
| 4-130 | $C_{16-6-6}Br_2$, CTAB | 130 | 6 | 10.7 | 12.3 | 0.26 | 3.0 ± 0.7 | 220 | 530 |
| ZSM-5 | TPAOH | 170 | 2 | 11.0 | 14.3 | 0.02 | – | 5[b] | 375 |
| AlSi-MCM-41 | CTAB | 100 | 3 | 11.0 | – | 0.76 | 2.9 ± 0.2 | 890 | 950 |

**Note.** RM is designation for the reaction mixture, τ is the duration of HTT, $V_{micro}$ is the micropore volume, $V_{meso}$ is the mesopore volume, $D_{meso}$ is the mesopore diameter, $S_{meso}$ is the mesopore specific surface area, $S_{BET}$ is the total specific surface area; [a]micropore diameter for the samples given in Table 1 is 0.55 nm, [b]external specific surface area of zeolite ZSM-5.

for zeolite formation, while the hydrophobic tails of this template limit the growth of Zt crystals and facilitate the formation of mesostructure. The synthesis conditions in the dual template synthesis in the presence of molecular and micellar templates favorable for the formation of zeolites and MMS are a reaction medium without alkali metal cations, low pH, relatively low temperature (~100 °C), and short hydrothermal treatment (HTT) [6]. Thus, it appeared favorable to carry out the synthesis of X-ray-amorphous and partially zeolitized MMAS using reaction mixtures without alkali metal cations; zeolite formation in such mixtures is possible at relatively low temperatures. In turn, the use of a micellar template combined with a dual functional template opens the possibility of additional and more precise regulation of the phase composition of the zeolitic MMAS (not containing an amorphous phase) as well as their structure and acidity, which, to a significant extent, determine the catalytic activity of these materials.

In the present work, we attempted to explain the effect of structure and acidity of micro-mesoporous alumosilicates derived from zeolite ZSM-5 obtained by the dual template method and using dual functional templates on their catalytic activity in cumene cracking as a test reaction: $C_6H_5C_3H_7 \rightarrow C_6H_6 + C_3H_6$.

## EXPERIMENTAL

MMAS samples 1-100-4-100 (Table 1) were obtained by the dual template method using sols containing ZSM-5 precursors (Si/Al = 50 in the starting reaction mixture). The synthesis of the MMAS was carried out using a reaction mixture with the composition $1.0SiO_2 : 0.01Al_2O_3 : 0.36$TPAOH $: 0.102$CTACl $: 16.27H_2O$ with tetrapropylammonium hydroxide (TPAOH) and cetytrimethylammonium chloride (CTACl) as the molecular and micellar templates respectively. Tetraethyl

orthosilicate (TEOS) was used as the source of silicon and aluminum nitrate nonahydrate was used as the source of aluminum. The dual template reaction mixture was subjected to HTT at 100 °C for 72 h (sample 1-100) or 144 h (sample 2-100) (Table 1). During preparation of samples 3-100 and 4-100, the pH of the sol precursor was lowered to 11.5 and 11.0, respectively, by the addition of 1.6 M hydrochloric acid. Then, the dual template reaction mixture was subjected to HTT at 100 °C for 72 h. A detailed description of the method of synthesis of samples 1-100-4-100 was given in our previous work [6].

A procedure similar to the method given by Choi et al. [7, 8] was used for the synthesis of MMAS (Si/Al = 50) in the presence of N,N′-dioctyl-N,N,N′,N′-tetramethyl-1,6-diammoniumhexane dibromide $[C_8H_{17}–N^+(CH_3)_2–C_6H_{12}–N^+(CH_3)_2–C_8H_{17}](Br^–)_2$ ($C_{8\text{-}6\text{-}8}Br_2$) and N-hexadecyl-N′-hexyl-N,N,N′,N′-tetramethyl-1,6-diammoniumhexane dibromide $[C_{16}H_{33}–N^+(CH_3)_2–C_6H_{12}\text{-}N^+(CH_3)_2–C_6H_{13}](Br^–)_2$ ($C_{16\text{-}6\text{-}6}Br_2$). The composition of the reaction mixture was $1.0SiO_2 : 0.01Al_2O_3 : 0.60NaOH : 0.10C_{8\text{-}6\text{-}8}Br_2$ ($C_{16\text{-}6\text{-}6}Br_2$) $: 0.24H_2SO_4 : 40H_2O$. The silicon source was silica sol Ludox HS-40 and the aluminum source was $Al_2(SO_4)\cdot 18H_2O$. When $C_{16\text{-}6\text{-}6}Br_2$ was used, the $H_2SO_4/SiO_2$ ratio was 0.18 and the silicon source was TEOS. In the synthesis of samples 1-130 (template $C_{8\text{-}6\text{-}8}Br_2$) and 3-130 ($C_{16\text{-}6\text{-}6}Br_2$), the starting reaction mixture was subjected to HTT at 130 °C for 144 h with stirring (rotation of the autoclave at ~60 rpm) (Table 1). The reaction mixture for obtaining MMAS using a dual functional template and additive of micellar template (cetyltrimethylammonium bromide (CTAB)) was prepared by dissolving $C_{8\text{-}6\text{-}8}Br_2$ and CTAB (sample 2-130) or $C_{16\text{-}6\text{-}6}Br_2$ and CTAB (sample 4-130) in an alkaline solution (the micellar template/dual functional template ratio was $1.3\cdot 10^{-3}$). Then, the synthesis was carried out in accord with the procedure described by Choi et al. [7, 8].

The procedure of Laugel et al. [9] was used to obtain zeolite ZSM-5 (Si/Al = 50). The MMS AlSi-MCM-41 (Si/Al = 50) was prepared by a common procedure [10].

All the samples were detemplated at 550 °C for 5 h. After detemplating, the Na-forms of samples 1-130-4-130, ZSM-5, and AlSi-MCM-41 were converted to the H-form by ion exchange with 1 M aqueous ammonium chloride and subsequent calcination at 550 °C for 5 h.

The phase composition of the resultant samples was analyzed using a Bruker AXS D8 ADVANCE X-ray diffractometer with Cu$K_\alpha$ radiation. The mean diameter of the ZSM-5 crystallites was calculated using the Scherrer equation. The degree of zeolitization was evaluated relative to the change in the ratio of the intensities of characteristic reflections at $2\theta = 23.0°$, 23.8°, and 24.2° of samples 1-100-4-100 and zeolite ZSM-5. The IR spectra of the samples in KBr pellets (1 : 100) were recorded on a Perkin Elmer Spectrum One Fourier transform spectrometer. The microphotographs of the samples were obtained on a JEOL JEM-2100F transmission electron microscope (TEM). The silicon and aluminum contents in the samples were determined by energy dispersive X-ray spectroscopy using an attachment to the JEM-2100F TEM. The solid-state $^{27}Al$ NMR spectra were taken on a Bruker Avance III 400WB spectrometer. The chemical shifts were determined relative to $Al(H_2O)_6Cl_3$ (1 M aqueous solution), $\delta = 0$ ppm. Nitrogen adsorption was measured by a volumetric method at 77 K up to 1 atm on Thermo electron Corp. Sorptomatic 1990 porous material analyzer. The samples were initially evacuated at $p \le 0.7$ Pa at 350 °C for 5 h. The total specific surface area ($S_{BET}$) was determined using the BET equation. The micropore diameter was found using the Saito–Foley method and the mesopore diameter was found by the BJH method. The volume of the micropores and mesopores as well as the specific surface area of the mesopores, which also includes the external specific surface area, for samples 1-130-4-130, was found by the comparative *t*-plot method. The volume of the zeolite ZSM-5 micropores was determined using the Dubinin–Radushkevich equation.

The acid properties of the samples were studied by a standard method of temperature-programmed desorption of ammonia (TPDA) [11]. The generally-accepted method of ad(de)sorption of pyridine with IR-spectral control was used to characterize the nature, strength, and concentration of acid sites [7, 12].

The catalytic cracking of cumene on these samples was carried out at atmospheric pressure and 300-400 °C (25 °C steps) in a micropulse mode using helium as the gas carrier. The samples were first activated at 500 °C for 1 h in a helium stream. A Tsvet-104 chromatograph with a flame ionization detector and a packed column containing 5 wt.% active phase XE-60 on Inerton AW-10-dimethyldichlorosilane as the solid phase was used to analyze the cracking products.

The yield of the reaction products $Y_i$ (wt.%) was calculated using the following formula:

$$Y_i = \frac{A_i}{\sum A_i} \cdot 100$$

where $A_i$ is the area of the $i$-th peak and $\sum A_i$ is the total area of the peaks of all the products. The value was converted to a molar value:

$$Y_i^{\text{mol}} = \frac{Y_i / M_i}{\sum \frac{Y_i}{M_i}} \cdot 100$$

where $Y_i^{\text{mol}}$ is the product yield, mole % and $M_i$ is the molar mass of the product, g/mol.

The cumene conversion ($X$) was calculated as the sum of the yields of the reaction products (mole %). The selectivity relative to each of the reaction products (mole %) was calculated using the formula

$$S_i = \frac{Y_i^{\text{mol}}}{X} \cdot 100.$$

**RESULTS AND DISCUSSION**

Using the X-ray diffraction data, the HTT of the reaction mixture containing TEOS and aluminum nitrate along with TPAOH and CTACl at 100 °C for 3-6 days leads to the formation of X-ray-amorphous sample 1-100 (Table 1) and partially zeolitized samples 2-100 (0.15 zeolitization), 3-100 (0.25), and 4-100 (0.05) having spatially-ordered mesostructure (Fig. 1a,b). The structure of sample 1-100 contains secondary ZSM-5 structural units, as indicated by the presence of IR absorption bands at ~550 $cm^{-1}$ assigned to asymmetric stretching vibrations of the (alumo)siloxane bonds of the five-membered rings of $Si(Al)O_{4/2}$ tetrahedra [13].

Agglomerates of ZSM-5 nanoparticles are formed in the reaction mixtures with dual functional template $C_{8\text{-}6\text{-}8}Br_2$ upon HTT at 130 °C for six days (Fig. 1a,b, sample 1-130). The nanoparticle diameter calculated using the TEM data and the Scherrer equation was ~35 nm (Fig. 1c). The presence of the small-angle reflection in the diffractogram of this sample shown in Fig. 1a indicates high homogeneity in size and shape of the zeolite nanoparticles, which is in accord with the results of Liu et al. [14]. The use of $C_{8\text{-}6\text{-}8}Br_2$ and CTAB as an additive (the CTAB concentration in the reaction mixture was 0.18 mmol/L, which is 5 times less than the first critical micelle concentration ($CMC_1$), limiting the growth of zeolite crystals, leads to a decrease in the ZSM-5 nanoparticle diameter from 35 to 27 nm (using the Scherrer equation) in the resultant alumosilicate (sample 2-130).

The use of dual functional template $C_{16\text{-}6\text{-}6}Br_2$ with HTT at 130 °C for six days gave sample 3-130 (Fig. 1a,b) consisting of randomly oriented flake-like particles, which are packets of ZSM-5 layers with layer thickness ~2 nm in the direction of crystallographic axis $b$ and total thickness 10-40 nm (TEM data (Fig. 1d)). The lamellar mesostructure of this sample is disordered after the template removal (Fig. 1a). The addition of CTAB to the reaction mixture containing $C_{16\text{-}6\text{-}6}Br_2$ (the CTAB concentration was 5 times less than $CMC_1$) facilitates formation of alumosilicate 4-130 (Fig. 1b) with a disordered lamellar mesostructure, which is resistant to detemplating. A reflection at $2\theta = 1.3°$, $d_0 = 6.7$ nm appears in the small-angle region (Fig. 1a). The zeolite layers in the lamellar mesostructure with thickness 2-3 nm are arranged at some angle.

MMAS samples 1-100-4-100 contain mesopores, which are rather homogeneous in size ($V_{\text{meso}}$ = 0.50-0.60 $cm^3/g$, diameter $D_{\text{meso}}$ = 2.3-2.7 nm, specific surface area $S_{\text{meso}}$ = 770-1240 $m^2/g$ (Table 1)). Partially zeolitized MMAS 2-100-4-100 also have small micropore fractions (Table 1). MMAS 1-130-4-130 have greater micropore volume ($V_{\text{micro}}$ = 0.11-0.14 $cm^3/g$, $D_{\text{micro}}$ = 0.55 nm (Table 1)) than the values found for samples 2-100-4-100 and have interparticle mesopores, which are relatively homogeneous in size ($V_{\text{meso}}$ = 0.26-0.41 $cm^3/g$, $D_{\text{meso}}$ = 2.5-11.0 nm, $S_{\text{meso}}$ = 500-540 $m^2/g$) and correspond to the space between the zeolite nanoparticles agglomerated during the synthesis. The addition of the micellar CTAB template to the reaction mixture enhances the values of $S_{\text{BET}}$ and $S_{\text{meso}}$ in the products (samples 2-130 and 4-130) and improved size homogeneity of the mesopores (Table 1).

The TPDA data indicate that the X-ray-amorphous sample 1-100 (Si/Al = 33) containing a ZSM-5 precursor and MMAS 4-100 (Si/Al = 44) with low zeolitization degree (0.05) contain medium-strength acid sites in concentration 90-154 μmol $NH_3/g$ or relative to a $S_{\text{BET}}$ unit 0.09-0.12 μmol $NH_3/m^2$ and display an ammonia desorption shoulder with maximum at 320 °C (Table 2). MMAS sample 2-100 (Si/Al = 27) with 0.15 zeolitization also contains strong acid sites

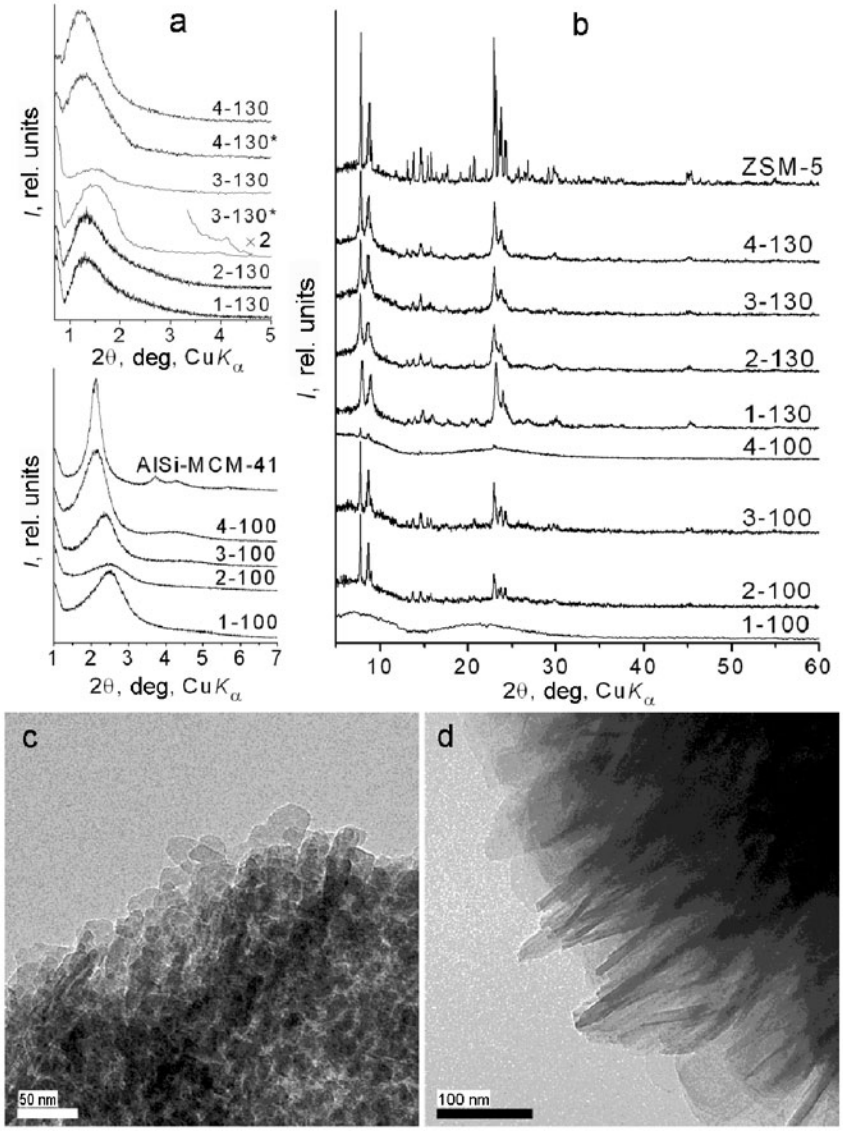


Fig. 1. Diffractograms of MMAS samples (the asterisks indicate non-detemplated samples), ZSM-5, and AlSi-MCM-41 in the small-angle (a) and medium-angle regions (b) and TEM microphotographs of samples 1-130 (c) and 3-130 (d).

(ammonium desorption maximum at 450 °C) in addition to the medium-strength acid sites with ammonia desorption maximum at 350 °C. An increase in zeolitization degree up to 0.25 (sample 3-100, Si/Al = 40) leads to an increase in the concentration of strong acid sites in the MMAS (Table 2). The data of ad(de)sorption of pyridine with IR-spectral control (Table 2) show that the concentration of Lewis acid sites in the samples 1-100-4-100 is 1.5-2 times greater than the concentration of Brønsted acid sites (pyridine is almost completely desorbed from these sites at 350 °C). Zeolitic MMAS 1-130-4-130 (Si/Al = 34-44) contain strong acid sites (Table 2, TPDA data) similar to zeolite ZSM-5 (Si/Al = 40). These samples show stronger Brønsted acid sites and higher concentrations (pyridine is completely desorbed from these sites at 450 °C) and a higher ratio of Brønsted acid sites to Lewis acid sites (2.6-3.7) than for samples 1-100–4-100 (Table 2).

X-ray-amorphous sample 1-100 displays greater catalytic activity in cumene cracking in the entire studied temperature range (300-400 °C, the cumene conversion is 52-91 mole % (Fig. 2a)) than AlSi-MCM-41 (34-67 mole %). This behavior is

TABLE 2. Si/Al Ratio in the Prepared Samples and Their Acidity by TPDA and Ad(de)sorption of Pyridine with IR-Spectral Control

| Sample | Si/Al in sample | TPDA acidity | | BAS, μmol/g (μmol/m$^2$)* | LAS, μmol/g (μmol/m$^2$)* |
|---|---|---|---|---|---|
| | | Temperature of $NH_3$ desorption maximum, °C | *C*, μmol/g (μmol/m$^2$)* | | |
| 1-100 | 33 | 210 | 60 (0.05) | 74 (0.06) | 149 (0.12) |
| | | 320 | 154 (0.12) | | |
| 2-100 | 27 | 200 | 102 (0.11) | 46 (0.05) | 95 (0.10) |
| | | 350 | 81 (0.08) | | |
| | | 450 | 17 (0.02) | | |
| 3-100 | 40 | 225 | 120 (0.14) | 48 (0.06) | 91 (0.11) |
| | | 440 | 38 (0.04) | | |
| 4-100 | 44 | 205 | 47 (0.05) | 70 (0.07) | 97 (0.10) |
| | | 320 | 90 (0.09) | | |
| 1-130 | 34 | 210 | 200 (0.40) | 148 (0.29) | 52 (0.10) |
| | | 440 | 196 (0.39) | | |
| 2-130 | 36 | 195 | 145 (0.27) | 74 (0.14) | 20 (0.04) |
| | | 425 | 173 (0.32) | | |
| 3-130 | 41 | 215 | 185 (0.37) | 129 (0.25) | 51 (0.10) |
| | | 440 | 159 (0.31) | | |
| 4-130 | 44 | 195 | 100 (0.19) | 71 (0.13) | 25 (0.05) |
| | | 425 | 145 (0.27) | | |
| ZSM-5 | 40 | 210 | 170 (0.45) | 113 (0.30) | 14 (0.04) |
| | | 440 | 136 (0.36) | | |
| AlSi-MCM-41 | 37 | 275 | 34 (0.04) | 30 (0.03) | 44 (0.05) |
| | | 320 | 26 (0.03) | | |

**Note.** BAS) concentration of Brønsted acid sites, LAS) concentration of Lewis acid sites, *) the concentration of acid sites per $S_{BET}$ unit is given in parentheses.

attributed to the higher concentration of medium-strength acid sites for sample 1-100 containing a ZSM-5 precursor than for AlSi-MCM-41 as indicated by the TPDA data (Table 2). Sample 4-100 with low zeolitization degree (0.05), which contains medium-strength acid sites (Table 2), also has greater catalytic activity in the temperature range 300-400 °C than for AlSi-MCM-41 (Fig. 2a). With increasing zeolitization of the MMAS from 0.05 for sample 4-100 to 0.15 for sample 2-100, we find a sharp increase in the cumene conversion, which is especially pronounced at lower reaction temperatures (Fig. 2a). This behavior occurs because partially zeolitized sample 2-100 has stronger acid sites (Table 2) than for samples 4-100 and 1-100. An increase in cumene conversion at 300 °C is observed upon a further increase in the zeolitization of the MMAS up to 0.25 (sample 3-100) and, as a consequence, an increase in the concentration of strong acid sites from 17 to 38 μmol $NH_3$/g (Fig. 2a).

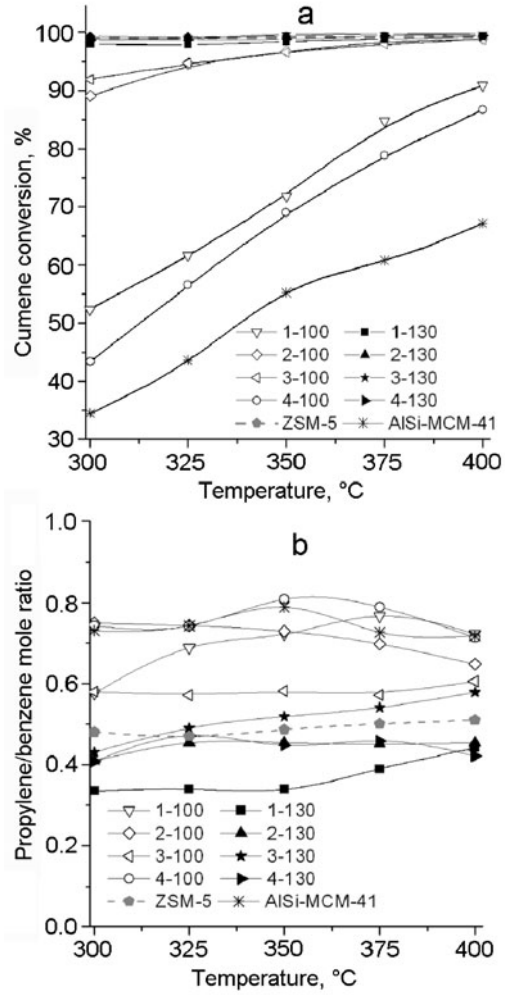


Fig. 2. Temperature dependence of cumene conversion (a) and the propylene/benzene molar ratio (b) for samples of MMAS, ZSM-5, and AlSi-MCM-41.

At higher temperatures (325-400 °C), the catalytic activity of partially zeolitized samples 2-100 and 3-100 is comparable to zeolite ZSM-5 (Fig. 2a). Samples 1-130-4-130, which have strong acid sites (Table 2), display high activity in cumene cracking in the temperature range 300-400 °C (Fig. 2a) similar to zeolite ZSM-5 and partially zeolitized samples 2-100 and 3-100.

The major cracking products on all studied samples are propylene and benzene, which are formed upon the dealkylation of cumene by the action of strong Brønsted acid sites [15]. Similar values for propylene selectivity (39-45 mole %) and benzene selectivity (55-60 mole %) as well as the propylene/benzene molar ratio (0.70-0.80 (Fig. 2b)) were found for samples 1-100, 2-100, 4-100, and AlSi-MCM-41 over the entire studied temperature range. Raising the zeolitization degree from 0.15 (for sample 2-100) to 0.25 (sample 3-100) leads to an increase in benzene selectivity (for example, this value increases from 57 to 63 mole % at 300 °C) and decrease in the propylene selectivity (from 42 to 36 mole %) and propylene/benzene molar ratio (from 0.75 to 0.58 (Fig. 2b)). These results indicate greater oligomerization of propylene on MMAS 3-100, whose products remain on the sample as coke precursors [16, 17]. This behavior may be attributed to the circumstance that sample 3-100 has a higher concentration of strong acid sites (Table 2, according to TPDA), which may favor coke formation [18] and greater fractions of micropores in the total adsorption volume ($V_{micro}/(V_{micro} + V_{meso}) = 0.05$) in comparison with sample 2-100 (0.02 micropore fraction). Propylene is retained more strongly in the micropores related to the zeolite phase than in the mesopores due to the greater adsorption potential and higher concentration of strong acid sites. Zeolite

MMAS 1-130-4-130, which possess a significant fraction of micropores (0.25-0.32) and high concentration of strong Brønsted acid sites (Table 2) similar to ZSM-5, display higher benzene selectivity (67-72 mole % at 300 °C) and lower propylene selectivity (24-29 mole % with propylene/benzene molar ratio 0.34-0.43) in comparison with samples 1-100-4-100 and AlSi-MCM-41.

Ethylbenzene, toluene, and styrene were found among the cumene cracking side-products. Toluene and ethylbenzene may be formed upon the disproportionation of cumene [15, 16, 19] involving Lewis acid sites. Styrene is formed as the result of the disproportionation of cumene on Lewis acid sites [19]. Toluene and ethylbenzene may also be formed through a monomolecular mechanism upon the protonation of cumene at the carbon atom adjacent to the ring bearing the isopropyl group and at the tertiary carbon atom of this group, respectively [20, 21].

X-ray-amorphous sample 1-100, partially zeolitized samples 2-100-4-100, and AlSi-MCM-41 display less total selectivity relative to the reaction side-products (0-2 mole %) in comparison with zeolitic MMAS samples 1-130-4-130 and ZSM-5 (5-6 mole %). This finding indicates that the side-product selectivity increases with increasing concentration and strength of the acid sites in our MMAS samples (Table 2, TPDA data), which was supported by the results of Bielanski and Malecka [22].

The same tendency was observed for the series of partially zeolitized samples. Sample 4-100 with only 0.05 zeolitization and AlSi-MCM-41, which contain medium-strength Brønsted and Lewis acid sites (Table 2), selectively convert cumene into propylene and benzene (trace amounts of toluene and ethylbenzene are formed in the presence of AlSi-MCM-41 only at 375-400 °C). The toluene and ethylbenzene selectivities for X-ray-amorphous sample 1-100, which has a higher concentration of medium-strength acid sites in comparison with sample 4-100 and AlSi-MCM-41 (Table 2, TPDA data) and MMAS samples 2-100 and 3-100, which contain strong as well as medium-strength acid sites, are higher but do not exceed 2 mole % over the entire studied temperature range.

On the other hand, zeolitic MMAS samples 1-130-4-130 display somewhat lower toluene and ethylbenzene selectivities at 300-400 °C (1-2 mole %) in comparison to ZSM-5 (up to 3 mole %). This discrepancy may be related to the lower concentration of Brønsted acid sites in the former samples (0.13-0.29 μmol Py/$m^2$) compared to ZSM-5 (0.30 μmol Py/$m^2$) (Table 2).

In some cracking temperature ranges, the partially zeolitized samples (2-100 and 3-100) and zeolitic MMAS 1-130-4-130 display higher styrene selectivity (up to 2 mole %) than for zeolite ZSM-5 (less than 1 mole %). This discrepancy is attributed to the well-developed specific surface area of the mesopores in these MMAS samples (Table 1), which facilitates the disproportion of cumene to give styrene and cymene with participation of the Lewis acid sites (hydride ion acceptors) [19]. This reaction in the micropores of ZSM-5 is sterically hindered.

Special interest has arisen in the finding that X-ray-amorphous sample 1-100 obtained using a zeolite sol precursor has a higher concentration of medium-strength Brønsted and Lewis acid sites in comparison to AlSi-MCM-41 with a similar Al/Si ratio (Table 2) and, as a consequence, displays greater catalytic activity in cumene cracking (Fig. 2a) than MMS. This finding was supported by the results of Huang et al. [23], who showed that an X-ray-amorphous alumosilicate isolated from the reaction mixture of BEA as well as MMS derived the sol precursor of this zeolite contain medium-strength acid sites (the ammonia desorption maximum is at 360 °C) and have greater catalytic activity (cumene conversion 70-90 mole %) than AlSi-MCM-41 (50 mole %). We may assume that the higher acidity and, as a consequence, greater catalytic activity of alumosilicate 1-100 are due to the higher concentration of tetrahedrally-coordinated aluminum in the zeolite precursors contained in this alumosilicate (the fraction of aluminum atoms in sample 1-100 in tetrahedral coordination is 72% and the fraction in octahedral coordination is 28% as shown by $^{27}$Al NMR spectroscopy) than in the amorphous framework of AlSi-MCM-41 (the fraction of aluminum in tetrahedral coordination is only 40%).

Thus, partially zeolitized MMAS derived from zeolite ZSM-5 (zeolitization degree 0.15-0.25), containing medium-strength and strong Brønsted and Lewis acid sites and a small fraction of micropores, display high catalytic activity in the cumene cracking approaching the activity of ZSM-5 and are superior to ZSM-5 in total selectivity relative to the major products, namely, propylene and benzene. The activity in this reaction increases with increasing fraction of micropores in the total alumosilicate porosity and increasing concentration of strong Brønsted acid sites along with a decrease in the propylene/benzene molar ratio in the reaction products. This result indicates more extensive oligomerization of the olefin in the zeolitic MMAS and ZSM-5 in comparison with AlSi-MCM-41, X-ray-amorphous alumosilicate containing zeolite precursors, and partially zeolitized MMAS.

**REFERENCES**


1. T. Prasomsri, W. Jiao, S. Z. Weng, and J. Garcia Martinez, *Chem. Commun.*, **51**, No. 43, 8900-8911 (2015).
2. N. D. Shcherban and V. G. Ilyin, *Teor. Éksp. Khim.*, **51**, No. 6, 331-349 (2015). [*Theor. Exp. Chem.*, **51**, No. 6, 339-357 (2015) (English translation).]
3. K. Na and G. A. Somorjai, *Catal. Lett.*, **145**, No. 1, 193-213 (2014).
4. Y. Liu and T. J. Pinnaviaia, *J. Mater. Chem.*, **12**, No. 11, 3179-3190 (2002).
5. M. Choi, K. Na, J. Kim, et al., *Nature*, **461**, No. 7261, 246-249 (2009).
6. R. Barakov, N. Shcherban, and P. Yaremov, et al., *J. Mater. Sci*., **51**, No. 8, 4002-4020 (2016).
7. K. Kim, R. Ryoo, H.-D. Jang, and M. Choi, *J. Catal.*, **288**, 115-123 (2012).
8. K. Na, M. Choi, W. Park, et al., *J. Am. Chem. Soc.*, **132**, No. 12, 4169-4177 (2010).
9. G. Laugel, X. Nitsch, F. Ocampo, and B. Louis, *Appl. Catal. A*, **402**, Nos. 1/2, 139-145 (2011).
10. N. Nishiyama, Y. Egashira, and K. Ueyama, *Mesoporous Silica, Mesoporous Silica Composite Material and Processes for the Production Thereof*, USA Patent 0232841, C 01 B 33/20, B 32 B 9/00, Publ. October 20, 2005.
11. S. Hu, J. Shan, Q. Zhang, et al., *Appl. Catal. A*, **445/446**, 215-220 (2012).
12. C. A. Emeis, *J. Catal.*, **141**, No. 2, 347-354 (1993).
13. C. E. A. Kirschhock, R. Ravishankar, F. Verspeurt, et al., *J. Phys. Chem. B*, **103**, No. 24, 4965-4971 (1999).
14. B. Liu, Y. Tan, Y. Ren, et al., *J. Mater. Chem.*, **22**, No. 35, 18631-18638 (2012).
15. A. Corma and B. W. Wojciechowski, *Catal. Rev.*, **24**, No. 1, 1-65 (1982).
16. A. Malecka, *J. Catal.*, **165**, No. 2, 121-128 (1997).
17. R. V. Likhn'ovskii, A. V. Yakovenko, and L. K. Patrilyak, et al., *Katal. Naftokhim.*, No. 7, 1-4 (2001).
18. J. Huang, Y. Jiang, V. R. R. Marthala, et al., *J. Catal.*, **263**, No. 2, 277-283 (2009).
19. D. Best and B. W. Wojciechowski, *J. Catal.*, **47**, No. 1, 11-27 (1977).
20. L. K. Patrilyak, *Katal. Neftekhim.*, No. 12, 16-20 (2003).
21. L. K. Patrilyak, *Katal. Naftokhim.*, No. 4, 16-18 (2000).
22. A. Bielanski and A. Malecka, *Zeolites*, **6**, No. 4, 249-252 (1986).
23. J. Huang, G. Li, S. Wu, et al., *J. Mater. Chem.*, **15**, No. 10, 1055-1060 (2005).